Photoacoustic Sentinel Lymph Node Imaging with Self-Assembled Copper Neodecanoate Nanoparticles

Dipanjan Pan,*,† Xin Cai,† Ceren Yalaz, Angana Senpan, Karthik Omanakuttan, Samuel A. Wickline, Lihong V. Wang,* and Gregory M. Lanza

C-TRAIN and Division of Cardiology, Washington University School of Medicine, 4320 Forest Park Avenue, St. Louis, Missouri 63108, United States, and Department of Biomedical Engineering, Washington University in St. Louis, One Brookings Drive, St. Louis, Missouri 63130, United States. †Equal contribution.

ABSTRACT Photoacoustic tomography (PAT) is emerging as a novel, hybrid, and non-ionizing imaging modality because of its satisfactory spatial resolution and high soft tissue contrast. PAT combines the advantages of both optical and ultrasonic imaging methods. It opens up the possibilities for noninvasive staging of breast cancer and may replace sentinel lymph node (SLN) biopsy in clinic in the near future. In this work, we demonstrate for the first time that copper can be used as a contrast metal for near-infrared detection of SLN using PAT. A unique strategy is adopted to encapsulate multiple copies of Cu as organically soluble small molecule complexes within a phospholipid-entrapped nanoparticle. The nanoparticles assumed a size of 80—90 nm, which is the optimum hydrodynamic diameter for its distribution throughout the lymphatic systems. These particles provided at least 6-fold higher signal sensitivity in comparison to blood, which is a natural absorber of light. We also demonstrated that high SLN detection sensitivity with PAT can be achieved in a rodent model. This work clearly demonstrates for the first time the potential use of copper as an optical contrast agent.

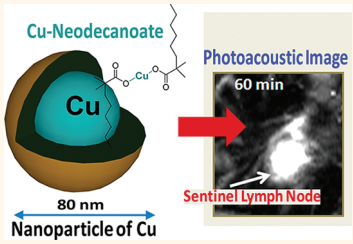

KEYWORDS: copper · nanoparticle · optical imaging · contrast agent · photoacoustic imaging · sentinel lymph node · breast cancer staging

Photoacoustic (PA) or optoacoustic imaging is a noninvasive technique that uniquely synergizes optical and ultrasound imaging.[1,2] The technique is based on a phenomenon in which the absorbed electromagnetic energy of light is transformed into kinetic energy and localized heating, releasing a pressure or radio frequency wave. The optical absorption can be associated with endogenous molecules, such as hemoglobin or melanin, or it can be achieved through exogenously delivered contrast agents, such as optical dyes, gold nanoparticles, or single-walled carbon nanotube (SWNT).[3—5] Due to the high concentration of hemoglobin (12 to 15 g/dL), blood inherently has a high magnitude of light absorption compared with surrounding tissues, which routinely allows blood vessels to be visualized. However, for PA imaging of nonvascular tissues (*e.g.*, lymph nodes) or intravascular biosignatures (*e.g.*, integrins), exogenous contrast agents must be employed. Of late, this hybrid imaging modality has been successfully used for breast cancer imaging, brain structural and functional imaging, blood oxygenation and hemoglobin monitoring, tumor angiogenesis, and, very recently, for detecting nascent angiogenic premature vessels in a rodent model.[6—10]

Breast cancer spreads to one or a few lymph nodes, the sentinel lymph node(s) (SLNs), before further metastasizing to other axillary nodes. Identification and sampling of SLN, known as sentinel node biopsy (SLNB), successfully reduced the need for complete axillary lymph node dissection and reduced the associated morbidities: lymphedema, nerve injury, and shoulder dysfunction. Consequently, SLNB has become widely practiced in the United States, Europe, and Australia. SLNB requires noninvasive detection of SLN, which are marked for intra-operative localization and resection with methylene blue dye placed preoperatively under imaging guidance. SLNB dye staining is approximately 90% effective, which can be improved to over 95% with radioactive colloid labeling, but the added expense and inconvenience of handling radioactive materials and performing intra-operative gamma imaging detracts from the technique.[11—16]

Interest in photoacoustic guided imaging for noninvasive axillary staging of breast cancer reflects the low cost and increased flexible convenience of preoperative and intraoperative imaging. In the absence of intrinsic PA contrast, exogenous contrast agents (*e.g.*, gold nanoparticles, indocyanine dye) must be employed to detect

* Address correspondence to dipanjan@wustl.edu (nanoparticle), lhwang@biomed.wustl.edu (photoacoustics).

Received for review October 10, 2011 and accepted January 9, 2012.

Published online January 09, 2012
10.1021/nn203895n

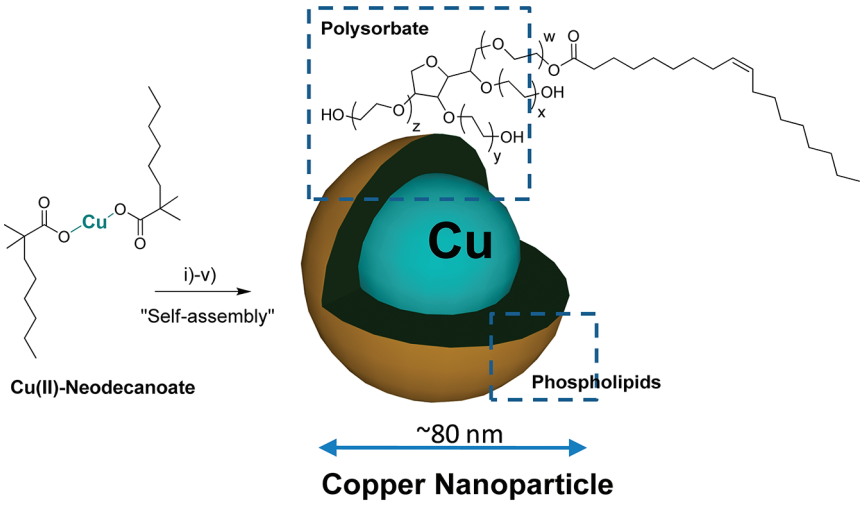

Physico-Chemical Characterization Table

Hydrodynamic diameter (D_h)= 86 ± 06 nm
Polydispersity index (PDI)= 0.21 ± 0.02
Zeta potential (ζ)= -12 ± 07 mV
Particle height (H_{av}) = 60 ± 14 nm
UV-vis spectroscopy = λ 603-746 nm
EDX = C 22 wt%, O 6 wt%, Cu 11 wt%
ICP-OES= 16.99 mg/L of Cu (20% colloidal suspension)

Figure 1. Synthesis and physicochemical characterization of self-assembled nanoparticles of copper neodecanoate. Schematic describing the preparation of copper-enriched nanoparticles: (i) suspension of copper neodecanoate (1) in sorbitan sesquioleate, vigorously vortex and mixing, filter using cotton bed, vortex; (ii) dissolve phospholipids in anhydrous chloroform and preparation of phospholipid thin film by slow evaporation of solvent at 45 °C under reduced pressure; (iii) resuspension of the thin film in water (0.2 μM); (iv) self-assenbly by high pressure homogenization at 4 °C, 20 000 psi (141 MPa), 4 min; (v) dialysis (cellulosic membrane, MWCO 20k); in box, characterization table for nanoparticles of copper neodecanoate.

lymph nodes. Recently, we[17] and other groups[18−21] have shown the utility of gold nanoparticles (≤90 nm) for enhancing SLN detection. However, the clinical use of gold is discouraged by the high and unpredicatable cost of the metal. Furthermore, the optical property of gold (*i.e.*, surface plasmon resonance) is dependent on expensive and complicated chemistries to tightly control particle surface coating and morphology. In this work, we hypothesized that copper-based nanoparticles could provide an innovative, inexpensive, and commercially viable alternative optical contrast agent for PA imaging. Copper is presently available at ~$20/kg in contrast to gold, which is being sold as a pure metal at $1800/oz. We have noted the use of previous PA contrast agents (approximately 50 nm), based on SWNT and gold nanoparticles (nanoshells, nanorods), which provided viable photoacoustic contrast in the near-infrared (NIR) region. However due to their "hard, crystalline" nature, the *in vivo* distribution and whole-body clearance is questionable and may create a regulatory barrier for clinical translation. To the best of our knowledge, the use of Cu for PA diagnostic imaging has never been reported.

Copper as a pure metal or mineral is abundant in the Earth's crust (~50 ppm) and historically available at low cost, particularly when compared with gold. In 1895, Cotton reported that the optical activity in bivalent copper complexes was largely dependent on the symmetry. Dissymmetry induced by d−d and d−p electronic mixings in different coordinations, such as octahedral, tetragonal, *etc.*, regulated the strength and the sign of optical rotation.[21] Both the absolute configuration of an asymmetric atom in a ligand and the asymmetry of the conformation of the chelate rings contribute to the overall optical activity of the system. We determined that a complex of Cu^{2+} with neodecanoic acid (NA) showed broad near-infrared (NIR) optical absorption, λ = ~600−700 nm, presumably due to crystal-field splitting as suggested by others.[22,23] Since the optical signal of hemoglobin occurs at λ = 500 nm, below the bandwidth of copper neodecanoate (CuNA), we hypothesized nanocolloids, rich in copper neodecanoate, could provide high PA contrast for sentinal lymph node imaging.

In the past, copper nanoparticles have been synthesized using various methods including high-temperature decomposition of organometallic precursors, supercritical carbon dioxide, *etc.*[21−25] Typically, these methods yield particles larger than the normal renal filtration threshold (*i.e.*, 6−10 nm), presenting long-term

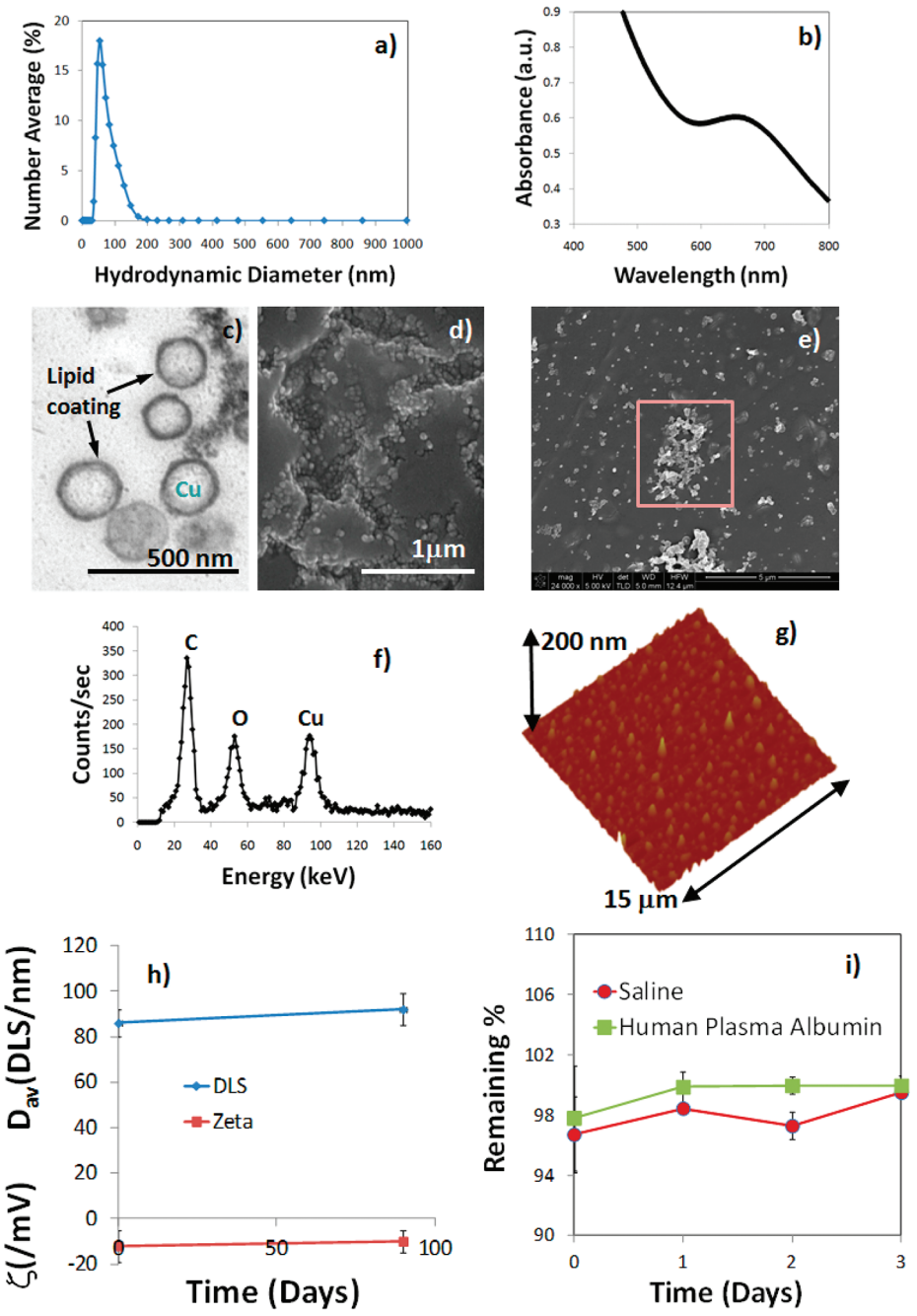

Figure 2. (a) Hydrodynamic particle size distribution from DLS; (b) UV−vis spectrum of NanoCuN nanoparticles in water; (c) anhydrous state TEM image; (d,e) SEM images; (f) EDX spectrum of the selected area from the image in (e); (g) AFM image (deposited on glass substrate); shelf life stability of NanoCuN over 90 days from formulation; (i) dissolution of Cu over 3 days when incubated with saline and human plasma albumin.

safety and regulatory challenges. Moreover, in contradistinction to usual "solid" or "hard" copper nanoparticle constructs, we developed a self-assembled "soft" particle synthesis derived from organically soluble Cu(II)-neodecanoate, with a targeted size of <90 nm, based on previous SLN optimization with gold nanobeacons.[17]

RESULTS AND DISCUSSION

Cu-neodecanoate complexes were mixed with polysorbates (sorbitan mono-9-octadecenoate poly (oxy-1,2-ethanediyl)) and encapsulated within a phospholipid outer layer. Polysorbate, a non-ionic surfactant derived from polyethoxylated sorbitan and oleic acid, is generally considered safe and often used in foods.[16] The hydrophilic groups in this compound were polyethers or polyoxyethylenes. CuNA was incorporated at 20% w/v within the polysorbate core matrix and encapsulated by 2% (v/v) phospholipids. The compatibility of CuNA with polysorbate allowed copper particle payloads of up to 60% (w/v). The surfactant mixture

comprised phosphatidylcholine (lecithin-egg PC, 50 mol %, Avanti Polar Lipids) and polysorbates (50 mol %). Briefly, the synthesis involved the vigorous mixing of Cu-neodecanoate (0.3 g) in toluene with polysorbate, followed by the evaporation of solvent from the mixture to produce a homogeneous suspension of CuNA in polysorbates at 80 °C under reduced pressure. This product was microfluidized as a 20% (v/v) colloidal suspension with 2% (v/v) phospholipid−polysorbate surfactant mixture in nanopure water (Figure 1). Nanoparticles were purified by exhaustive dialysis through 10 kDa MWCO membrane against deionized water (0.2 μM) (Figure 1) to remove any unbound copper. Nanoparticles of copper neodecanoate (NanoCuN) exhibited high shelf life stability at 4 °C with less than 5% change in particle sizes and polydispersity over 5 months. Dynamic light scattering measurements of NanoCuN revealed a hydrodynamic diameter of 86 ± 06 nm (D_h) with a low polydispersity (PDI) of 0.21 ± 0.02 (Brookhaven Instrument Co.). The negative electrophoretic potential value of −12 ± 07 mV suggests a complete and successful encapsulation of the copper−polysorbate core with surfactant.

Copper content determined by inductively coupled plasmon optical emission spectroscopy (ICP OES) was 16.99 mg/L of the 20% colloidal suspension. The measurement of the UV−vis spectrum of NanoCuN in water revealed optical absorption wavelengths (λ) between 603 and 746 nm (λ_{max} = 683 nm), which corroborated the presence of copper complexes. The particles were characterized in the anhydrous state by transmission electron microscopy (TEM), atomic force microscopy (AFM), energy-dispersive X-ray spectroscopy (EDX), and scanning electron microscopy (SEM). Using TEM, the uranyl acetate stained CuNPs were observed to be spherical with a distinct dark lipid periphery (Figure 2c). AFM particle height was 60 ± 14 nm. NanoCuN, diluted ~1:100× with acetone, was placed as a drop on a silicon wafer and allowed to air dry for SEM and EDX analyses. The SEM images (HV = 5 kV) confirmed the spherical morphology of the nanoparticles. Elemental analysis (HV = 5 kV) confirmed the presence of Cu within the sample (Figure 2f).

Copper is known to pose toxicity when used in high concentration. Therefore, it is important to establish the safety and stability of these particles prior to their *in vivo* use. These particles exhibited remarkable shelf stability with time and maintain the particle integrity for future clinical translation. Changes in hydrodynamic diameter and electrophoretic potential were monitored over a period of 90 days. Only insignificant variation was noticed when preserved under argon atmosphere at 4 °C (Figure 2i). The efficiency of the copper entrapment in the particle was tested in a dissolution experiment. The nanoparticle was incubated with saline and human plasma albumin at 37 °C, and the total release of the copper complex

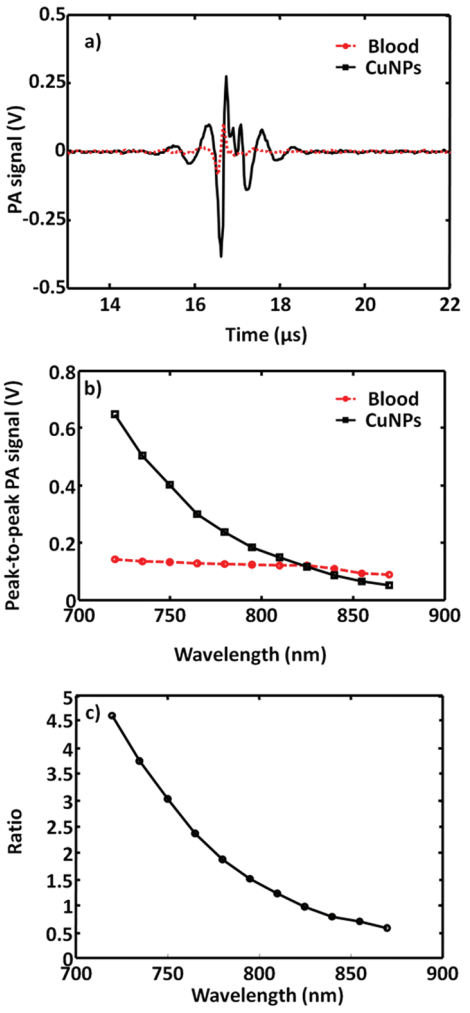

Figure 3. (a) PA spectroscopy signals generated from a tygon tube (i.d. = 250 μm, o.d. = 500 μm) filled with NanoCuN (20% colloidal suspension and rat blood). The laser was tuned to 720 nm wavelength. (b) Comparative PA spectra of NanoCuN and rat blood over a 720−870 nm NIR wavelength range. (c) Ratio of the peak-to-peak PA signal amplitudes generated from NanoCuN to those of blood over a range of 720−870 nm.

was measured over time. The release of the copper neodecanoate was monitored by UV−vis spectroscopy over the 600−750 nm wavelength range. Nanoparticles were shown to retain 96−97% of the complex with only <4% release over 3 days against an infinite sink (Figure 2j). These results confirm that copper is retained well in dissolution and no substantial *in vitro* release of copper was noticed.

Since hemoglobin is a dominant optical absorber in the human body and produces strong PA contrast, the efficacy of NanoCuN was first compared with blood in the NIR wavelength window. Figure 3a shows the PA signals obtained from a tygon tube (i.d. = 250 μm, o.d. = 500 μm) filled with CuNP (20 vol %) and whole rat blood (hematocrit ~45%; hemoglobin ~15 g/dL). Since the photoacoustic scanner is limited by the accessibility of laser wavelength at 670 nm, the laser was tuned to the closest excitation, λ = 720 nm. At this

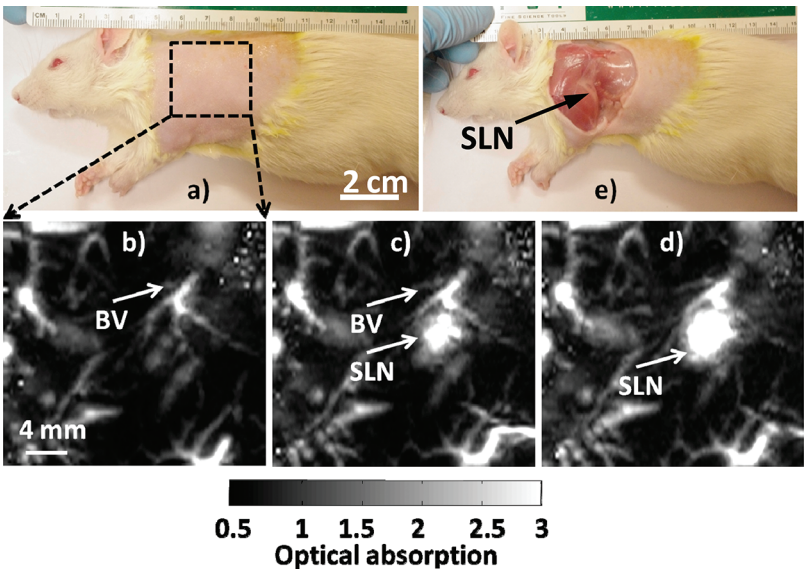

Figure 4. Noninvasive *in vivo* PA images (maximum intensity projections, MIP) of the SLN in a rat. (a) Photograph of the rat with region of interest depilated before scanning. The scanning region is delineated by a black dotted square. (b) Baseline PA image acquired before NanoCuN injection. Bright regions represent inherent optical absorption from a blood vessel (BV). (c) PA image (MIP) acquired almost immediately after NanoCuN administration. (d) PA image 60 min post-injection showing a marked signal enhancement corresponding to increased NanoCuN uptake by the node: Blood vessel (BV) and sentinel lymph node (SLN) are marked with arrows. The SLN is visible in both (c) and (d), however, not apparent in (b). (e) Photograph of the rat with the skin excised after PA imaging. For (b)−(d), FOV = 25 mm × 24 mm, step size along the *X* direction = 0.2 mm, step size along the *Y* direction = 0.4 mm, total scan time = ~23 min. No signal averaging was used.

wavelength, the peak-to-peak PA signal amplitude obtained from NanoCuN was ~650 mV, compared to ~140 mV peak-to-peak PA signal amplitude from blood alone. Figure 3b shows the PA spectrum (peak-to-peak PA signal amplitude *versus* excitation light wavelength) of the copper nanoparticles (in black) for an excitation wavelength range of 720−870 nm. The PA spectrum of rat blood (in red) is overlaid on the same figure. The PA signal obtained from NanoCuN was clearly much stronger than blood over the entire range of wavelengths. Figure 3c illustrates the ratio of the peak-to-peak PA signal amplitude of NanoCuN to that of blood between 720 and 870 nm. The PA signal from the tygon tube filled with copper nanoparticles is more than five times stronger than that from blood at 720 nm. Weak hemoglobin absorption within the NIR window is well-known and exploited for deep tissue PA imaging. A typical preparation of NanoCuN (Cu content: 16.99 mg/mL for a 20% colloidal suspension) provided a SNR of 42 dB at 720 nm wavelength *in vitro*. The noise equivalent concentration (*i.e.*, the concentration that provides a SNR of unity) is calculated to be ~0.4 mg/mL. The magnitude of PA signal derived from NanoCuN within the NIR region suggests potential clinical utility for both intravascular as well as extravascular diagnostic applications. PA signal of NanoCuN is approximately five times stronger than that of rat blood, which is either higher or comparable to gold nanoparticles in terms of the signal strength. Interestingly, in our previous work, gold nanobeacons (GNB)[17] provided 12-fold signal enhancement over blood at a concentration of 2 wt/vol % in contrast to 0.02% wt/vol % for the copper nanoparticles used in the present study. In addition, this platform presents the flexibility to optimize the metal loading and can easily be increased at least to 2 wt/vol %. More in depth study is warranted to understand comparative molar absorptivities and PA signal of the system, which is presently in progress in our laboratories.

Our previous work for gold nanocages demonstrated that the PA system could detect the SLN as deep as ~33 mm.[18−20] Figure 4a shows a representative digital photograph of a rat taken prior to image acquisition. The axillary skin was shaved prior to PA imaging. Before NanoCuN administration, a baseline (*i.e.*, control PA image) was obtained, which is presented as a maximum intensity projection (MIP, Figure 4b). The vasculature, denoted as BV, was sharply imaged (500 μm × 500 μm in-plane resolution), but no lymph node(s) were visible at baseline. However, as shown in Figure 4c, PA imaging of the same region of interest immediately after the NanoCuN injection into the paw prominently revealed the SLN not previously apparent; at 60 min post-injection (Figure 2d), the magnitude of PA contrast was further enhanced, reflecting a substantial increase in NanoCuN uptake by the draining SLN. Figure 4e presents a digital photograph of the same animal with the skin excised following the PA imaging experiment. Excised lymph node was analytically tested for copper by ICP-OES, which revealed the copper content to be 0.2415 mg/L, 60 min post-injection.

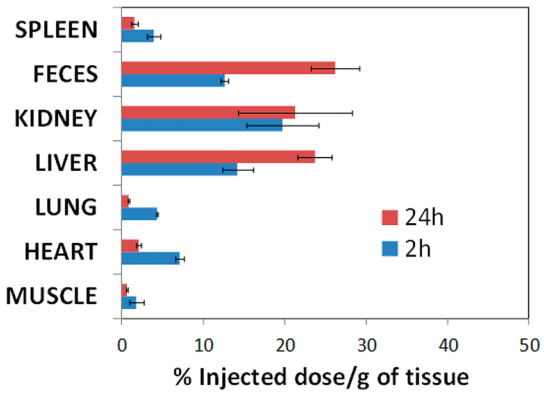

Figure 5. Preliminary biodistribution of NanoCuN in rats: distribution of copper (NanoCuN) in major organs determined by ICP-OES at 2 and 24 h following intravenous injection of nanoparticles (1 mg/mL of 20% colloidal suspension). Distribution of copper in major organs (liver, kidney, spleen, lung, heart, and muscle) is expressed as % injected dose/g of tissue.

The preliminary biodistribution of these particles was studied in a rat model. Following intravenous injection (1 mL/kg, 20 vol % of nanoparticles), animals ($n = 2$) were sacrificed at 2 and 24 h post-injection. The major organs (*i.e.*, liver, spleen, heart, lung, muscle, and kidney) were collected, weighed, and digested. The concentration of copper in the digested sample was determined by ICP-OES (Figure 4a). Results indicate anticipated clearance of the particle through the reticuloendothelial system (RES) as marked by the high copper accumulation in spleen, liver, and kidney. Kidney and feces accumulated 19.7 ± 4.4 and 12.6 ± 0.5% injected dose (ID)/g of tissue, whereas liver and lung gathered 14.2 ± 1.9 and 4.3 ± 0.1% ID/g of tissue. Other major organs accumulated smaller amounts of NanoCuN at 2 h post-injection. Spleen, heart, and muscle accumulated 3.9 ± 0.8, 7.1 ± 0.5, and 1.8 ± 0.9% ID/g of tissue, respectively. At 24 h after NanoCuN injection, feces, liver, and kidney accumulated 26.2 ± 3, 23.7 ± 2.1, and 21.3 ± 7% ID/g of tissue, respectively (Figure 5), and were the major sites of nanoparticle buildup. Other major organs (*i.e.*, spleen, heart, and muscle) accumulated 1.6 ± 0.4, 2.1 ± 0.3, and 0.6 ± 0.1% ID/g of tissue, respectively, after 24 h post-injection. More comprehensive study to understand their *in vivo* distribution is presently in progress.

CONCLUSION

These data, for the first time, clearly demonstrate the potential use of copper as contrast agents for identification of SLNs with photoacoustic scanning systems. To the best of our knowledge, there is only one previous report of using copper sulfide nanoparticles as a photothermal agent.[26,27] Copper neodecanoate, by virtue of its unique optical properties within in the NIR range, provided substantial PA contrast and, in contradistinction to "hard" copper particle approaches, allowed facile synthesis of "soft" agents with stable, readily excreted small molecule complexes. Although there are reports of toxicity from copper,[28] the design of these nanoagents allowed us to incorporate hydrophobic copper complexes in a highly stable manner. NanoCuN produced nearly five times more signal than blood as a 20% colloidal suspension. NanoCuN offered rapid sentinel lymph node detection in rats in comparison to gold nanorods. At a concentration of 1 μM, gold nanorods (10 nm in diameter and 41 nm in length) were shown to follow a much slower kinetics in the rodent model and took more than 20 h to be observed at SLNs.[19] These results suggest that enhanced sentinel lymph node PA imaging is possible with nanoparticles of copper neodecanoate.

METHODS

Unless otherwise listed, all solvents and reagents were purchased from Aldrich Chemical Co. (St. Louis, MO) and used as received. Anhydrous chloroform was purchased from Aldrich Chemical Co. and distilled over calcium hydride prior to use. High purity egg yolk phosphatidylcholine was purchased from Avanti Polar Lipids, Inc. Cholesterol and sorbitan sesquioleate were purchased and used as received from Aldrich Chemical Co. (St. Louis, MO). Cu(III)-neodecanoate was purchased from Spectrum Chemicals, Inc. and used as received. Argon and nitrogen (UHP, 99.99%) were used for storage of materials. The Spectra/Por membrane (Cellulose MWCO = 10 000 Da) used for dialysis was obtained from Spectrum Medical Industries, Inc. (Laguna Hills, CA).

Preparation of Copper Neodecanoate Nanoparticles. NanoCuN was prepared by suspending copper neodecanoate (0.3 g in 60% toluene, Aldrich Chemicals, Inc.) in sorbitan mono-9-octadecenoate poly(oxy-1,2-ethanediyl) (5 mL, Aldrich Chemicals, Inc.) and vigorously vortexing the mixture to homogeneity. The toluene was evaporated off under reduced pressure at 80 °C. The surfactant co-mixture included high purity egg yolk phosphatidylcholine (80 mol %, 281 mg) and sorbitan mono-9-octadecenoate poly(oxy-1,2-ethanediyl) (20 mol %, 124 mg). The surfactant co-mixture was dissolved in chloroform, evaporated under reduced pressure, dried in a 50 °C vacuum oven overnight, and dispersed into water by probe sonication. This suspension was combined with the copper polysorbate mixture (20% v/v), distilled, deionized water (77.3% w/v), and glycerin (1.7%, w/v). The mixture is continuously processed thereafter at 20 000 psi for 4 min with an S110 Microfluidics emulsifier. The nanoparticles were dialyzed against water using a 10 000 Da MWCO cellulose membrane for a prolonged period of time and then passed through a 0.45 μm Acrodisc syringe filter. The nanoparticles were stored under argon atmosphere typically at 4 °C in order to prevent any bacterial growth. DLS (D_{av})/nm = 86 ± 06 nm; aeta (ζ)/mV = −12 ± 05 mV; TEM (D_{ah})/nm = 97 ± 30; AFM (H_{av})/nm = 60 ± 14 nm, PDI = 0.22 ± 0.02; UV−vis spectroscopy (λ_{max}) = 603−746 nm; ICP-OES = 16.99 mg of Cu/L.

Dynamic Light Scattering Measurements. Hydrodynamic diameter distribution and distribution averages for the copper nanoparticles in aqueous solutions were determined by dynamic light scattering. Hydrodynamic diameters were determined using a Brookhaven Instrument Co. (Holtsville, NY) model Zeta Plus particle size analyzer. Measurements were made following dialysis (MWCO 10 kDa dialysis tubing, Spectrum

Laboratories, Rancho Dominguez, CA) of NanoCuN in deionized water (0.2 mM). Nanoparticles were dialyzed into water prior to analysis. Scattered light was collected at a fixed angle of 90°. A photomultiplier aperture of 400 mm was used, and the incident laser power was adjusted to obtain a photon counting rate between 200 and 300 kcps. Only measurements for which the measured and calculated baselines of the intensity autocorrelation function agreed to within +0.1% were used to calculate nanoparticle hydrodynamic diameter values. All determinations were made in multiples of five consecutive measurements.

Electrophoretic Potential Measurements. Electrophoretic (zeta) potential (*z*) values for the NanoCuN were determined with a Brookhaven Instrument Co. (Holtsville, NY) model Zeta Plus zeta-potential analyzer. Measurements were made following dialysis (MWCO 10 kDa dialysis tubing, Spectrum Laboratories, Rancho Dominguez, CA) of NanoCuN suspensions into water. Data were acquired in the phase analysis light scattering (PALS) mode following solution equilibration at 25 °C. Calculation of *z* from the measured nanoparticle electrophoretic mobility (ζ) employed the Smoluchowski equation: $\mu = \varepsilon\zeta/\eta$, where ε and η are the dielectric constant and the absolute viscosity of the medium, respectively. Measurements of ζ were reproducible to within ±4 mV of the mean value given by 16 determinations of 10 data accumulations.

Stability of the Nanocolloids. Long-term shelf stability of the nanocolloids was assessed by measuring hydrodynamic diameter distributions over a period of >60 days from the time of synthesis for different replicates of YbNC formulations preserved under inert atmosphere (*i.e.*, argon) at 4 °C. Changes in particle size and polydispersity indexes due to Ostwald ripening were minimal (<7%) over the observation period.

Inductively Coupled Plasma Optical Emission Spectroscopy. The copper (Cu) content of NanoCuN was analyzed by inductively coupled plasma optical emission spectroscopy (ICP-OES, Perkin-Elmer Optima 7000). The samples were treated with a mixture of concentrated nitric acid, concentrated hydrochloric acid, and hydrogen peroxide followed by digestion using Multiwave 3000 (Anton Paar, USA).

Animal Studies. Guidelines on the care and the use of laboratory animals at Washington University in St. Louis were followed for all animal experiments. Initial anesthetization of rat was done using a mixture of ketamine (85 mg/kg) and xylazine (15 mg/kg) and maintained on 0.75−1.0% isoflurane delivered through a calibrated vaporizer. NanoCuN was administered (1 mL/kg; total volume) intravenously through tail vein catheter. The major organs were independently frozen, ground to tissue homogeneity, weighed, digested, and the entire specimen was analyzed for Cu content using ICP-OES.

Photoacoustic Spectroscopy. *Light source:* tunable Ti:sapphire 443 laser (720−870 nm), LT-2211A, LOTIS TII) pumped by a Q-switched Nd:YAG (LS- 2137/2, LOTIS TII); pulse width <15 ns, pulse repetition rate 10 Hz. The incident laser fluence on the sample surface was controlled to conform to the American National Standards Institute standards. *Transducer:* 5 MHz central frequency, spherically focused, 2.54 cm focul length; 1.91 cm diameter active area element, 72% bandwidth (V308, Panametrics-NDT); low-noise amplifier (5072PR, Panametrics-NDT). Data were acquired with a digital oscilloscope (TDS 5054, Tektronix).

Acknowledgment. This research was supported by grants from the AHA (0835426N and 11IRG5690011), NIH (R01CA154737), NCI (U54CA119342), BRP (HL073646), and the NHLBI (R01HL073646, R01HL078631). We thank Mr. Allen J. Stacy for help with the biodistribution experiment. We also thank Ms. Marilyn Levy (Cell Biology) and Ms. Kate Nelson (Nano Research Facility, Washington University in St. Louis) for helping us with TEM and EDX experiments, respectively.

REFERENCES AND NOTES

1. Wang, X. D.; Pang, Y. J.; Ku, G.; Xie, X. Y.; Stoica, G.; Wang, L. H. V. Noninvasive Laser-Induced Photoacoustic Tomography for Structural and Functional *In Vivo* Imaging of the Brain. *Nat. Biotechnol.* **2003**, *21*, 803–806.
2. Wang, X. D.; Xie, X Y.; Ku, G.; Wang, L. H. V. Noninvasive Imaging of Hemoglobin Concentration and Oxygenation in the Rat Brain Using High-Resolution Photoacoustic Tomography. *J. Biomed. Opt.* **2006**, *11*, 024015.
3. Li, M. L.; Oh, J. T.; Xie, X. Y.; Ku, G.; Wang, W.; Li, C.; Lungu, G.; Stoica, G.; Wang, L. H. V. Simultaneous Molecular and Hypoxia Imaging of Brain Tumors *in Vivo* Using Spectroscopic Photoacoustic Tomography. *Proc. IEEE* **2008**, *96*, 481–489.
4. de la Zerda, A.; Zavaleta, C.; Keren, S.; Vaithilingam, S.; Bodapati, S.; Liu, Z.; Levi, J.; Smith, B. R.; Ma, T.-J.; Oralkan, O.; Cheng, Z.; Chen, X.; Dai, H.; Khuri-Yakub, B. T.; Gambhir, S. S. Carbon Nanotubes as Photoacoustic Molecular Imaging Agents in Living Mice. *Nat. Nanotechnol.* **2008**, *3*, 557–562.
5. Pan, D.; Pramanik, P.; Senpan, A.; Yang, X.; Song, K. H.; Scott, M. S.; Zhang, H.; Gaffney, P. J.; Wickline, S. A.; Wang, L. V.; Lanza, G. M. Molecular Photoacoustic Tomography with Colloidal Nanobeacons. *Angew. Chem., Int. Ed.* **2009**, *48*, 4170–4173.
6. Song, K. H.; Stein, E. W.; Margenthaler, J. A.; Wang, L. H. V. Noninvasive Photoacoustic Identification of Sentinel Lymph Nodes Containing Methylene Blue *in Vivo* in a Rat Model. *J. Biomed. Opt.* **2008**, *13*, 054033.
7. Pramanik, M.; Song, K. H.; Swierczewska, M.; Green, D.; Sitharaman, B.; Wang, L. H. V. *In Vivo* Carbon Nanotube-Enhanced Non-invasive Photoacoustic Mapping of the Sentinel Lymph Node. *Phys. Med. Biol.* **2009**, *54*, 3291–3301.
8. Song, K. H.; Kim, C. H.; Cobley, C. M.; Xia, Y. N.; Wang, L. H. V. Near-Infrared Gold Nanocages as a New Class of Tracers for Photoacoustic Sentinel Lymph Node Mapping on a Rat Model. *Nano Lett.* **2009**, *9*, 183–188.
9. Kim, J. W.; Galanzha, E. I.; Shashkov, E. G.; Moon, H. M.; Zharov, V. P. Golden Carbon Nanotubes as Multimodal Photoacoustic and Photothermal High-Contrast Molecular Agents. *Nat. Nanotechnol.* **2009**, *4*, 688–694.
10. Pan, D.; Pramanik, M.; Senpan, A.; Allen, J. S.; Zhang, H.; Wickline, S. A.; Wang, L. V.; Lanza, G. M. Molecular Photoacoustic Imaging of Angiogenesis with Integrin-Targeted Gold Nanobeacons. *FASEB J.* **2011**, *25*, 875–882.
11. Cady, B.; Stone, M. D.; Schuler, J. G. The New Era in Breast Cancer. Invasion, Size, and Nodal Involvement Dramatically Decreasing as a Result of Mammographic Screening. *Arch. Surg.* **1996**, *131*, 301–308.
12. Haffty, B. G.; Ward, B.; Pathare, P. Reappraisal of the Role of Axillary Lymph Node Dissection in the Conservative Treatment of Breast Cancer. *J. Clin. Oncol* **1997**, *15*, 691–700.
13. Veronesi, U.; Paganelli, G.; Viale, G. A Randomized Comparison of Sentinel-Node Biopsy with Routine Axillary Dissection in Breast Cancer. *N. Engl. J. Med.* **2003**, *349*, 546–553.
14. Krag, D.; Weaver, D.; Ashikaga, T.; Moffat, F.; Klimberg, V. S.; Shriver, C.; Feldman, S.; Kusminsky, R.; Gadd, M.; Kuhn, J.; Harlow, S.; Beitsch, P. The Sentinel Node in Breast Cancer—A Multicenter Validation Study. *N. Eng. J. Med.* **1998**, *339*, 941–946.
15. Ung, O. A. Australasian Experience and Trials in Sentinel Lymph Node Biopsy: The RACS SNAC Trial. *Asian J. Surg.* **2004**, *27*, 284–290.
16. Purushotham, A. D.; Upponi, S.; Klevesath, M. B.; Bobrow, L.; Millar, K.; Myles, J. P.; Duffy, S. W. Morbidity after Sentinel Lymph Node Biopsy in Primary Breast Cancer: Results from a Randomized Controlled Trial. *J. Clin. Oncol.* **2005**, *23*, 4312–4321.
17. Pan, D.; Pramanik, M.; Senpan, A.; Ghosh, S.; Wickline, S. A.; Wang, L. V.; Lanza, G. M. Near Infrared Photoacoustic Detection of Sentinel Lymph Nodes with Gold Nanobeacons. *Biomaterials* **2010**, *31*, 4088–4093.
18. Kim, C.; Song, K. H.; Gao, F.; Wang, L. V. Sentinel Lymph Nodes and Lymphatic Vessels: Noninvasive Dual-Modality *in Vivo* Mapping by Using Indocyanine Green in Rats—Volumetric Spectroscopic Photoacoustic Imaging and Planar Fluorescence Imaging. *Radiology* **2010**, *255*, 442–450.
19. Song, K. H.; Kim, C.; Maslov, K.; Wang, L. H. V. Noninvasive *In Vivo* Spectroscopic Nanorod-Contrast Photoacoustic

Mapping of Sentinel Lymph Nodes. *Eur. J. Radiol.* **2009**, *70*, 227–231.
20. Cai, X.; Li, W.; Kim, C. H.; Yuan, Y.; Wang, L. V.; Xia, Y. *In vivo* quantitative evaluation of the transport kinetics of gold nanocages in a lymphatic system by noninvasive photoacoustic tomography. *ACS Nano* **2011**, *5*, 9658–9667.
21. Lisiecki, I.; Pileni, M. P. Synthesis of Copper Metallic Clusters Using Reverse Micelles as Microreactors. *J. Am. Chem. Soc.* **1993**, *115*, 3887–3896.
22. Bigall, N. C.; Hartling, T.; Klose, M.; Simon, P.; Eng, L. M.; Eychmuller, A. Monodisperse Platinum Nanospheres with Adjustable Diameters from 10 to 100 nm: Synthesis and Distinct Optical Properties. *Nano Lett.* **2008**, *8*, 4588–4592.
23. Link, S.; El-Sayed, M. A. Size and Temperature Dependence of the Plasmon Absorption of Colloidal Gold Nanoparticles. *J. Phys. Chem. B* **1999**, *103*, 4212–4217.
24. Crouse, C.; Barron, A. R. Reagent Control over the Size, Uniformity, and Composition of Co−Fe−O Nanoparticles. *J. Mater. Chem* **2008**, *18*, 4146–4153.
25. Williams, G. L.; Vohs, J. K.; Brege, J. J.; Fahlman, B. D. Supercritical Fluid Facilitated Growth of Copper and Aluminum Oxide Nanoparticles. *J. Chem. Educ.* **2005**, *82*, 771–774.
26. Li, Y.; Lu, W.; Huang, Q.; Huang, M.; Li, C.; Chen, W. Copper Sulfide Nanoparticles for Photothermal Ablation of Tumor Cells. *Nanomedicine* **2010**, *5*, 1161–1171.
27. Melancon, M. P.; Zhou, M.; Li, C. Cancer Theranostics with Near-Infrared Light-Activatable Multimodal Nanoparticles. *Acc. Chem. Res.* **2011**, *44*, 947–956.
28. Brewer, G. J. Copper Toxicity in the General Population. *Clin. Neurophysiol.* **2010**, *121*, 459–460.